

---

# LEARNING STOCHASTIC DIFFERENTIAL EQUATIONS USING RNN WITH LOG SIGNATURE FEATURES

---

A PREPRINT

Shujian Liao

Department of Mathematics,  
University College London  
ucahiao@ucl.ac.uk

Terry Lyons

Mathematical Institute,  
University of Oxford  
terry.lyons@maths.ox.ac.uk\*  
Hao Ni

Weixin Yang

Mathematical Institute,  
University of Oxford  
weixin.yang@maths.ox.ac.uk†

Department of Mathematics,  
University College London‡  
h.ni@ucl.ac.uk

December 21, 2024

## ABSTRACT

This paper contributes to the challenge of learning a function on streamed multimodal data through evaluation. The core of result of our paper is the combination of two quite different approaches to this problem. One comes from the mathematically principled technology of signatures and log-signatures as representations for streamed data, while the other draws on the techniques of recurrent neural networks (RNN). The ability of the former to manage high sample rate streams and the latter to manage large scale nonlinear interactions allows hybrid algorithms that are easy to code, quicker to train, and of lower complexity for given accuracy.

We illustrate the approach by approximating the unknown functional as a controlled differential equation. Linear functionals on solutions of controlled differential equations are the natural universal class of functions on data streams. They are mathematically very explicit and interpretable, allow quantitative arguments, and yet are able to approximate any continuous function on streams arbitrarily well. They form the basis of rough path theory. Stochastic differential equations are examples of controlled differential equations where the controlling stream is a stochastic process. Following this approach we give a hybrid Logsig-RNN algorithm that learns functionals on streamed data with outstanding performance.

## 1 Introduction

The relationship between neural networks and differential equations is an active area of research ([39], [25], [4]). For example, Funahashi et al. introduced the continuous recurrent neural network(RNN) [13]; He et al. connect residual networks and discretized ODEs [39]. A typical continuous RNN has the form

$$\dot{Y}_t = -\frac{Y_t}{\tau} + A\sigma(BY_t) + I_t, \quad (1)$$

---

\*TL is supported by the EPSRC under the program grant EP/S026347/1 and by the Alan Turing Institute under the EPSRC grant EP/N510129/1.

†WY is supported by Royal Society Newton International Fellowship.

‡HN is supported by the EPSRC under the program grant EP/S026347/1 and by the Alan Turing Institute under the EPSRC grant EP/N510129/1.

where  $I_t$  and  $Y_t$  are an input and output at time  $t$  respectively<sup>4</sup>. Rough Path Theory teaches us that is more robust to consider the differential equation of the type

$$dY_t = V(Y_t)dX_t, \tag{2}$$

and replace  $I$  as an input with its integral. We can rewrite (1) in this form by setting  $X_t = (t, \int_{s=t_0}^t I_s ds)$  and  $V(y, (t, x)) = -\frac{y}{\tau}t + A\sigma(By)t + x$ . This allows the input to be of a broader type, and  $X$  need not even be differentiable for the equation to be well defined.  $Y$  inherits its regularity from  $X$ ; equations in this form admit uniform estimates when  $X$  is a rough path (highly oscillatory and potentially non-differentiable). This reformulation provides a much broader class of mathematical models for functionals on streamed data, of which the continuous RNN is a special case.

In [28] Lyons gives a deterministic pathwise definition to Equation (2) driven by rough signals. This analysis applies to almost all paths of e.g. vectored valued Brownian motion, diffusion processes, and also to many processes outside the SDE case, paths rougher than semi-martingales. [28] articulates that in order to control the solution to Equation (2), it suffices to control the  $p$ -variation and the iterated integrals of  $X$  (the *signature* of  $X$ ) up to degree  $[p]$ . Crucially these estimates allow  $p \gg 1$  and allow accurate descriptions of  $Y_t$  to emerge from the coarse global descriptions of  $X$  and its oscillations given by the signature. The *log-signature* carries the exactly the same information as the signature but is considerably more parsimonious; it is a second mathematically principled transformation, and like the signature, it is able to summarize and vectorize complex un-parameterized streams of multi-modal data effectively over a *coarse* time scale with a *low dimensional* representation.

One area where this has been worked out in detail is with the numerical analysis of stochastic differential equations (SDEs). The most effective high order numerical approximation schemes for SDEs show that describing a path through the log-signature enables one to effectively approximate the solution to the equation and any linear functional of that solution globally over interval the path is defined on, without further dependence on the fine details of the *recurrent structure* of the streamed data. It leads (in what is known as the log-ode method) to state of the art numerics.[?]We exploit this understanding to propose a simply but surprisingly effective neural network module (Logsig-RNN) by blending the Log-signature (Sequence) Layer with the RNN layer (see Figure 1) as an universal model for functionals on un-parameterized (and potentially complex) streamed data.

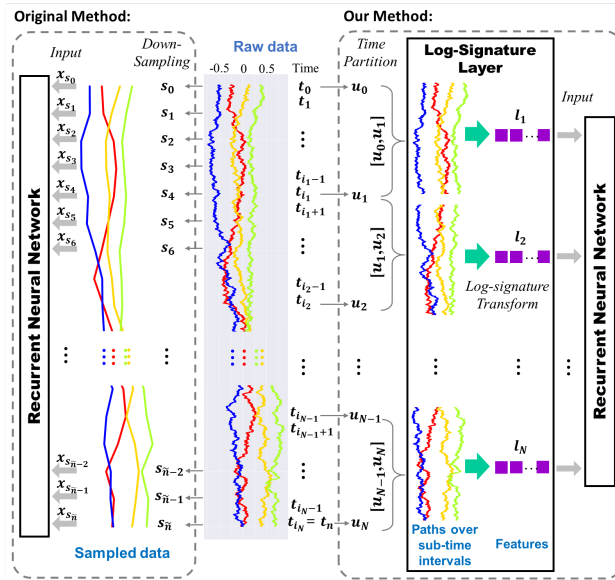


Figure 1: Comparison of Logsig-RNN and RNN.

The Logsig-RNN network has the following advantages:

1. **Time Dimension Reduction:** The Log-signature Layer transforms a time series to a sequence of the log-signatures over a potentially much coarser time partition. It reduces the time dimension of RNN significantly and thus speed up the backpropogation through time in training.
2. **High Frequency and Continuous data:** For the typical high frequency streamed data case, the RNN type approach suffers from severe limitation, when applied directly[9]. In this case, one has to down-sample the

<sup>4</sup> $\tau$  is a constant,  $A$  and  $B$  are matrices and  $\sigma$  is an activation function.

stream data to a coarser time grid to feed it into the RNN-type algorithm (Figure 1 (Left)). It may miss the microscopic characteristic of the streamed data and render lower accuracy. The logsig-RNN model can tackle such case or even continuous data streams very well (Figure 1).

3. **Highly Oscillatory Stream data:** There is a fundamental issue when one accesses a highly oscillatory stream through sampling. It is quite possible for two streams to have very different effects and yet have near identical values when sampled at very fine levels [11]. Therefore, to model a functional on a general highly oscillatory stream, the RNN on the sampled stream data would be challenged, requiring huge amounts of augmentation, and very fine sampling to be effective. In contrast, the rough path theory shows that if one postulates the (log)-signature of streamed data up in advance, the Logsig-RNN model can be much effective.

In summary, the main contributions of the paper are listed as follows:

1. to introduce the Log-signature (Sequence) Layer as a transformation of sequential data, and outline its back-propagation through time algorithm. It is highlighted that the Log-signature Layer can be inserted between other neural network layers conveniently, not limited to the pre-defined feature extraction.
2. to design the novel neural network model (Logsig-RNN model) by blending the log-signature layer with RNN (Section 3.2) and prove the universality of the Logsig-RNN model for the approximation any solution map to the SDEs (Theorem 4.2);
3. to propose the LP-Logsig-RNN model by adding the linear project layer in front of the Logsig-RNN architecture to tackle the case for the high dimensional input path (Section 3.3).
4. to apply the Logsig-RNN algorithm to both synthetic data and empirical data to demonstrate its superior accuracy, effectiveness and robustness (Section 5). We achieve the state-of-the-art classification accuracy 92.21% on ChaLearn2013 gesture data by the LP-Logsig-RNN model (Section 5.3).

## 1.1 Related Work

### 1.1.1 Learning SDEs

SDEs of the form (2) are useful tools for modelling random phenomena and provide a general class of functionals on the path space. SDEs not only are commonly used as models for the time-evolving process of many physical, chemical and biological systems of interacting particles [14], but also are the foundational building blocks in the derivatives pricing theory, an area of huge financial impact ([2], [29], [7]). Statistical inference for SDEs has rich literature due to the importance of research outcomes and applications (see [1] for the survey and overview). Most of the research focuses on the parameter estimation of (model-specific) stochastic processes; in particular [33] is the pioneering work for the parameter estimation for a general stochastic process, which goes beyond diffusion processes by matching expected signature of the solution process. However, in contrast to these work, our approach is non-parametric and is used to learn the solution map without any assumption on the distribution of the stochastic process.

### 1.1.2 Rough paths theory in machine learning

Recently the application of the rough path theory in machine learning has been an emerging and active research area. The empirical applications of the rough paths theory primarily focused on the *signature* feature, which serves as an effective feature extraction, e.g. online handwritten Chinese character/text recognition([15], [40]), action classification in videos [41], and financial data analysis ([16], [27]). In addition, those previous work mainly combine the signature with the convolutional neural network or fully connected neural network. To our best knowledge, the proposed method is the first of the kind to integrate the sequence of log signature with the RNN. The log-signature brings many benefits (Section 2.3). The log-signature has been used as a local feature descriptor for gesture [22] and action recognition [41]. These used cases are bespoke; in contrast, the proposed Logsig-RNN is a general method for sequential data with outstanding performance in various datasets (See Section 5). Moreover, we extend the work on the back-propagation algorithm of the log-signature transformation in [34] to the *sequence* of the log-signature.

### 1.1.3 Time series modelling

In [21] Levin et al. firstly proposed the signature of a path as the basis functions for a functional on the unparameterized path space and suggested the first non-parametric model for time series modelling by combining signature feature and the linear model (Sig-OLR). However, Sig-OLR has the limitation of inefficient global approximation due to the instability of the polynomial extrapolation. Despite the successful empirical applications of the signature feature sets ([15], [40], ([41])), the theoretical question on which learning algorithms are most appropriate to be

combined with the (log)-signature feature remains open. Our work is devoted to answering this question with both theoretical justification and promising numerical evidence.

### 1.1.4 Functional Data Analysis

Learning a functional on streamed data falls under the category of the functional data analysis (FDA) [31], which models data using functions or functional parameters and analyse data providing information about curves, surfaces or anything else varying over a continuum. The representation theory of the functional on functions plays an important role in FDA study. Functional principal components analysis ([36]) is one of the main techniques of FDA to represent the function data, which express the function data as the linear coefficients of the basis functions(usually without taking into account the response variable corresponding to the function input). In contrast to it, albeit taking the functional view of sequential data, our approach focuses on the representation of the path in terms of its effect (functional on the path, i.e. the solution of the controlled differential equation driven by the path).

## 2 Preliminary

In the following, let  $E := \mathbb{R}^d$  and  $X : J \rightarrow E$  be a continuous path endowed with a norm denoted by  $|\cdot|$ , where  $J = [S, T]$ .

### 2.1 A Path with finite $p$ -variation

In order to make precise about the class of paths we discuss throughout the paper, we introduce the  $p$ -variation as a measure of the smoothness of the path.

**Definition 2.1** ( $p$ -Variation). *Let  $p \geq 1$  be a real number. Let  $X : J \rightarrow E$  be a continuous path. The  $p$ -variation of  $X$  on the interval  $J$  is defined by*

$$\|X\|_{p,J} = \left[ \sup_{\mathcal{D} \subset J} \sum_{j=0}^{r-1} |X_{t_{j+1}} - X_{t_j}|^p \right]^{\frac{1}{p}}, \quad (3)$$

where the supremum is taken over  $\mathcal{D} = (t_1, t_2, \dots, t_r)$ , which is any possible subdivision of  $J$ <sup>5</sup>.

Let  $V_p(J, E)$  denote the range of any continuous path mapping from  $J$  to  $E$  of finite  $p$ -variation. The  $p$ -variation of a path represents the roughness of a path. The compactness of the time interval  $J$  can't ensure the finite 1-variation of a continuous path in general. We give a stochastic example in Example 2.1.

**Example 2.1.** *A fractional Brownian motion (fBM) with Hurst parameter  $H$  has sample paths of finite  $p$ -variation a.s. for  $p > \frac{1}{H}$ . For example, Brownian motion is a fBM with  $H = 0.5$ . It has finite  $(2 + \varepsilon)$ -variation a.s.  $\forall \varepsilon > 0$ , but it has infinite  $p$ -variation a.s. for any  $p \in [1, 2]$ .*

In practice, we may observe the discrete time series or the partial observations of the continuous path  $x$ , denoted by  $x^{\mathcal{D}} := [x_{t_1}, x_{t_2}, \dots, x_{t_r}]$ , where  $\mathcal{D} = (t_1, \dots, t_r)$ .  $\hat{\mathcal{D}}$  is reserved for the sampling time partition of raw data. To embed discrete time series into the path space brings the flexibility to describe sequential data in a unified way; it can help with the problem of missing data, time series of variable length and unequal spaced sampling. In the following discussion, we lift discrete time series to a path by interpolation (See detailed discussion in Section 4 of [21]). It is noted that the discrete version of a path  $x^{\mathcal{D}}$  is of finite 1-variation.

For each  $p \geq 1$ , the  $p$ -variation norm of a path  $X : J \rightarrow E$  of finite  $p$ -variation is denoted by  $\|X\|_{p-var}$  and defined as follows:

$$\|X\|_{p-var} = \|X\|_{p,J} + \sup_{t \in J} \|X_t\|.$$

### 2.2 The signature of a path

In this section, we introduce the signature and the log signature of a path, which takes values in the tensor algebra space denoted by  $T((E))$  endowed with the tensor multiplication and componentwise addition[26].

<sup>5</sup> Let  $J = [S, T]$  be a closed bounded interval where  $0 \leq S < T$ . A partition or a subdivision of  $J$  is an increasing sequence of real numbers  $\mathcal{D} = (t_0, t_1, \dots, t_r)$  such that  $0 < S \leq t_0 < t_1 < \dots < t_r < T$ . Let  $|\mathcal{D}|$  denote the number of time points in  $\mathcal{D}$ , i.e.  $|\mathcal{D}| = r + 1$ .  $\Delta\mathcal{D}$  denotes the time mesh of  $\mathcal{D}$ , i.e.  $\Delta\mathcal{D} := \max_{i=0}^{r-1} (t_{i+1} - t_i)$ .

**Definition 2.2** (The Signature of a Path). *Let  $J$  denote a compact interval and  $X : J \rightarrow E$  be a continuous path with finite  $p$ -variation such that the following integration makes sense. Let  $I = (i_1, i_2, \dots, i_n)$  be a multi-index of length  $n$  where  $i_j \in \{1, \dots, d\}, \forall j \in \{1, \dots, n\}$ . Define the coordinate signature of the path  $X_J$  associate with the index  $I$  as follows:*

$$X_J^I = \int \dots \int_{\substack{u_1 < \dots < u_k \\ u_1, \dots, u_k \in J}} dX_{u_1}^{(i_1)} \otimes \dots \otimes dX_{u_n}^{(i_n)}$$

The signature of  $X$  is defined as follows:

$$S(X)_J = (1, \mathbf{X}_J^1, \dots, \mathbf{X}_J^k, \dots) \quad (4)$$

$$\text{where } \mathbf{X}_J^k = \int \dots \int_{\substack{u_1 < \dots < u_k \\ u_1, \dots, u_k \in J}} dX_{u_1} \otimes \dots \otimes dX_{u_k} = (X_J^I)_{I=(i_1, \dots, i_k)}, \forall k \geq 1.$$

Let  $S_k(X)_J$  denote the truncated signature of  $X$  of degree  $k$ , i.e.

$$S_k(X)_J = (1, \mathbf{X}_J^1, \dots, \mathbf{X}_J^k). \quad (5)$$

**Example 2.2.** For  $X$  is a multi-dimensional Brownian motion, the above integration can be defined in both Stratonovich and Itô sense. It is because that the Brownian motion has samples of finite  $p$ -variation for only  $p > 2$  a.s., which results in defining the integration in a non-unique way.

The signature of the path has geometric properties. The first level signature  $\mathbf{X}_J^1$  is the increment of the path  $X$ , i.e.  $X_T - X_S$ , while the second level signature represents the signed area enclosed by the curve  $X$  and the cord connecting the ending and starting point of the path  $X$ .

The signature of  $X$  arises naturally as the basis function to represent the solution to linear controlled differential equation based on the Picard's iteration ([26]). It plays the role of non-commutative monomials on the path space. In particular, if  $X$  is a one dimensional path, the  $k^{\text{th}}$  level of the signature of  $X$  can be computed explicitly by induction as follows that for every  $k \in \mathbb{N}$ ,

$$\mathbf{X}_J^k = \frac{(X_T - X_S)^k}{k!}. \quad (6)$$

**Remark 2.1** (The Signature of Discrete Time Series). *It is important to note that  $S(x^{\mathcal{D}})$  is NOT the collection of all the monomials of discrete time series! The dimension of all monomials of  $x^{\mathcal{D}}$  grow with  $|\mathcal{D}|$ , while the dimension of  $S_k(x^{\mathcal{D}})$  is invariant to  $|\mathcal{D}|$ .*

The signature of a path has many good algebraic and analytic properties, which makes itself an efficient representation of an un-parameterized path. First of all, the signature of the path can recover the path trajectory under a mild condition.

**Theorem 2.1** (Uniqueness of the signature). *Let  $X \in V_p(J, E)$ . Then  $S(X)$  determines  $X$  up to the tree-like equivalence<sup>6</sup>. [3], [17]*

**Remark 2.2.** *A simple sufficient condition for the uniqueness of the signature of a path of finite length is that one component of  $X$  is monotone. Thus the signature of the time-joint path determines its trajectory (see [21]). For more details of the signature feature we refer to [5] and [26].*

Any functional on the path can be rewritten as a function on the signature based on the uniqueness of the signature (Theorem 2.1). The signature of the path has the universality, i.e. that any continuous functional on the signature can be well approximated by the linear functional on the signature (Theorem 2.2)[21].

**Theorem 2.2** (Signature Approximation Theorem). *Suppose  $f : S_1 \rightarrow \mathbb{R}$  is a continuous function, where  $S_1$  is a compact subset of  $S(V_p(J, E))$ <sup>7</sup>. Then  $\forall \varepsilon > 0$ , there exists a linear functional  $L \in T((E))^*$  such that*

$$\sup_{a \in S_1} \|f(a) - L(a)\| \leq \varepsilon. \quad (7)$$

We say that a path  $\tilde{X} : J \rightarrow E$  is the time re-parameterization of  $X : J \rightarrow E$  if and only if there exists a non-decreasing surjection  $\lambda : J \rightarrow J$  such that  $\tilde{X}_t = X_{\lambda(t)}, \forall t \in J$ .

<sup>6</sup>The rigorous definition of the tree-like path can be found in Definition A.2. Intuitively a tree-like path is a trajectory in which a section where the path exactly retraces itself.

<sup>7</sup> $S(V_p(J, E))$  denotes the range of the signature of  $x \in V_p(J, E)$ .

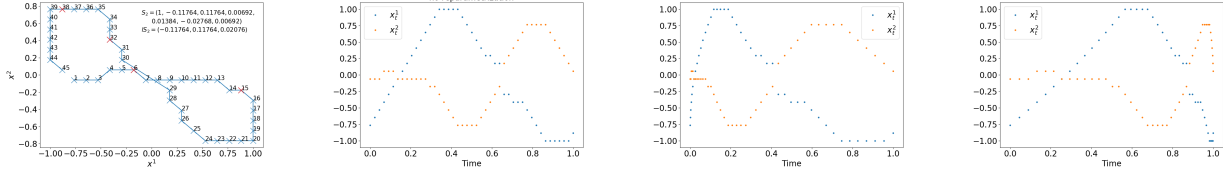


Figure 2: The top-left figure represents the trajectory of the digit 8, and the rest of figures plot the coordinates of the pen location via different speed respectively, which share the same signature and log signature given in the top right part of the first subplot.

**Lemma 2.1** (Invariance under time parameterization). [26] *Let  $X \in V_1(J, E)$  and a path  $\tilde{X} : J \rightarrow E$  is the time re-parameterization of  $X$ . Then*

$$S(X)_J = S(\tilde{X})_J. \quad (8)$$

Re-parameterizing a path inside the interval does not change its signature. In Figure 2, speed changes result in different time series representation but the same (log)signature feature. It means that signature feature can remove the redundancy caused by the speed of traversing the path, which brings massive dimension reduction to the application where the output is invariant with the speed of an input path, e.g. handwritten character recognition.

The signature feature set can deal with time series of variable length. For example, in Figure 3(Right) one pen trajectory sample is obtained by randomly throwing 5 points in Figure 3, which also results in unequal time spacing. Two samples in Figure 3 have the same dimension of their corresponding (log) signature.

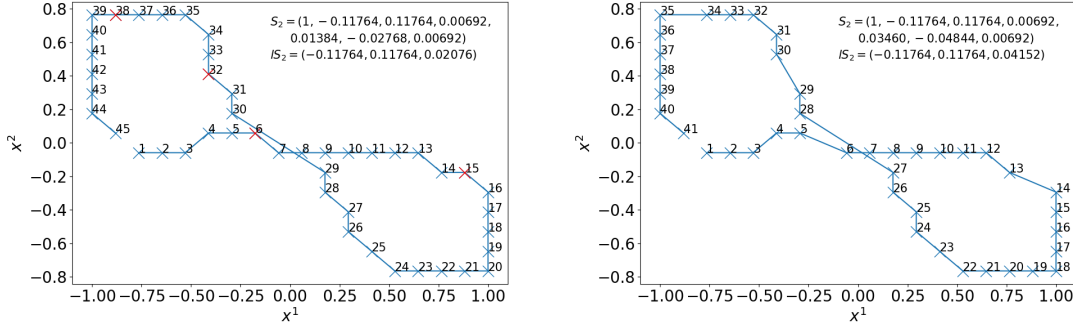


Figure 3: Figure(Right) is a path of handwritten digit 8 by randomly throwing away 4 points in pen trajectory of Figure(Left).  $\times$  represents pen location and the number associated with  $\times$  is its time index.  $\times$  represents the point thrown away of the pen trajectory in Figure (Left). The corresponding (log)-signature is given at the top-right part of figures.

### 2.3 The log-signature of a path

The logarithm of the element in  $T((E))$  is defined similar to the power series of the logarithm of a real value except for the multiplication is understood in the tensor product sense.

**Definition 2.3** (Logarithm map). *Let  $a = (a_0, a_1, \dots) \in T((E))$  be such that  $a_0 = 1$  and  $t = a - 1$ . Then the logarithm map denoted by  $\log$  is defined as follows:*

$$\log(a) = \log(1 + t) = \sum_{n=1}^{\infty} \frac{(-1)^{n-1}}{n} t^{\otimes n}, \forall a \in T((E)). \quad (9)$$

Similarly we have the exponential mapping of the element in  $T((E))$  defined in a power series form.

**Definition 2.4** (Exponential map). *Let  $a = (a_0, a_1, \dots) \in T((E))$ . Define the exponential map denoted by  $\exp$  as follows:*

$$\exp(a) = \sum_{n=0}^{\infty} \frac{a^{\otimes n}}{n!}. \quad (10)$$

**Lemma 2.2.** *The logarithm map is bijective on the domain  $\{a \in T((E)) \mid a_0 = 1\}$ . The inverse of the logarithm map is the exponential map.*

**Definition 2.5** (The Log Signature of a Path). *The log signature of path  $X$  by  $\log(S(X))$  is the logarithm of the signature of the path  $X$ , denoted by  $lS(X)$ . Let  $lS_k(X)$  denote the truncated log signature of a path  $X$  of degree  $k$ .*

**Remark 2.3.** *As the logarithm map is bijective, thus there is one-to-one correspondence between the signature and the log-signature [26]. The statement is also true for truncating the signature and log-signature up to the same degree. However, the log signature provides the parsimonious description of the signature, which is of lower dimension compared with the signature feature in general.*

By projecting both sides of Eqn (2.3) to  $E$ , the first level of signature and log-signature are both increments of the path  $X_T - X_S$ . For the second level of the signature  $(X^{i,j})_{i,j \in \{1,2\}}^d$ , it can be decomposed to its symmetric and anti-symmetric parts

$$X^{(i,j)} = \frac{1}{2}X^{(i)}X^{(j)} + A^{(i,j)}, \quad (11)$$

where

$$A_{S,T}^{(i,j)} = \frac{1}{2} \left( X^{(1,2)} - X^{(2,1)} \right). \quad (12)$$

It is noted that for  $i = j$ ,  $A^{(i,j)} = 0$  and  $lS_2 = A^{(1,2)}[e_1, e_2]$ . This is an example to show that the signature and log signature(lower dimension) is a bijection up to degree 2.

The log-signature has some algebraic property. Let us consider the linear subspace of  $T((E))$  equipped with the Lie bracket operation  $[\cdot, \cdot]$ , defined as follows:

$$[a, b] = a \otimes b - b \otimes a.$$

**Theorem 2.3.** (Theorem 2.3, [26]) *For any path  $X$  of finite 1-variation, there exist  $\lambda_{i_1, \dots, i_n}$  such that the log-signature of  $X$  can be expressed in the following form<sup>8</sup>*

$$lS(X) = \sum_{i=1}^d \lambda_i e_i + \sum_{n=2}^{\infty} \sum_{i_1, i_2, \dots, i_n \in \{1, 2, \dots, d\}} \lambda_{i_1, i_2, \dots, i_n} [e_{i_1}, [e_{i_2} \cdots, [e_{n-1}, e_n]]]. \quad (13)$$

If truncating the log-signature and signature to the same degree, the dimension of the log-signature is lower than that of the signature (except for the first degree, their dimensions are equal). It is because of the linear dependence of  $[e_{i_1}, [e_{i_2} \cdots, [e_{n-1}, e_n]]]$ . For example,  $[e_i, e_j] = -[e_j, e_i]$ .

Let summarize useful properties of the log-signature as a feature set of sequential data. As the one-to-one correspondence of the signature and lot-signature, the log-signature has the uniqueness of a path and the invariance of time parameterization. However, the log-signature has lower dimension than that of the signature, but the log-signature is NOT a basis of functional on a path. We summarize the comparison of the signature and log-signature in Table 1.

	signature	log-signature
uniqueness of a path	✓	✓
invariance of time parameterization	✓	✓
basis function	✓	✗
no redundancy	✗	✓

Table 1: Comparison of Signature and Log-signature

## 2.4 Recurrent Neural Network

The RNN is composed with three types of layers, i.e. the input layer  $(x_t)_t$ , the hidden layer  $(h_t)_t$  and the output layer  $(o_t)_t$ . RNN takes the sequence of  $d$ -dimensional vectors  $(x_1, x_2, \dots, x_T)$  as an input and compute the output  $(o_t)_{t=1}^T \in \mathbb{R}^{e \times T}$  using Equation (14):

$$h_t = \sigma(Ux_t + Wh_{t-1}), o_t = q(Vh_t), \quad (14)$$

where  $U, W$  and  $V$  are model parameters, and  $\sigma$  and  $q$  are two activation functions in the hidden layer and output layer respectively. Let  $\mathcal{R}_\sigma((x_t)_t \mid \Theta)$  denote the RNN model with  $(x_t)_t$  as the input,  $\sigma$  and linear function  $q$  as the activation functions of the hidden layer and output layer respectively and  $\Theta := \{U, W, V\}$  is the set of all the model parameters of the RNN model.

<sup>8</sup>Equivalently speaking, the log signature of a path is a Lie Series, which is defined in Definition A.1.

### 3 Logsig-RNN Network

#### 3.1 Log-Signature Layer

Consider a discrete  $d$ -dimensional time series  $x^{\mathcal{D}} = (x_{t_i})_{i=1}^n$ . The lifted path associated with  $x^{\mathcal{D}}$  is the piecewise linear interpolation of  $x^{\mathcal{D}}$ , which is a path of finite 1-variation. Thus its signature/log-signature are well defined. We define the Log-Signature (Sequence) Layer as follows.

**Definition 3.1** (Log-Signature (Sequence) Layer). *Let  $\hat{\mathcal{D}} := (t_k)_{k=0}^n$  and  $\mathcal{D} := (u_k)_{k=0}^N$  be two time partitions of  $J$  and  $\mathcal{D} \subset \hat{\mathcal{D}}$ . A Log-Signature Layer of degree  $M$  is a mapping from  $\mathbb{R}^d \times \mathbb{R}^n$  to  $\mathbb{R}^{d_{ls}} \times \mathbb{R}^N$ , which computes  $(l_k)_{k=0}^{N-1}$  as an output for any  $x^{\mathcal{D}}$ , where  $l_k$  is the truncated log signature of  $x$  over the time interval  $[u_k, u_{k+1}]$  of degree  $M$  as follows:*

$$l_k = lS_M(x_{[u_k, u_{k+1}]})$$

where  $k \in \{0, 1, \dots, N-1\}$  and  $d_{ls}$  is the dimension of the truncated log-signature.

It is noted that the Log-Signature Layer does not have any trainable weights. In addition, the input dimension of Log-signature layer is  $(d, n)$  and the output dimension is  $(N, d_{ls})$  where  $N \leq n$  and  $d_{ls} \geq d$ . The Log-Signature Layer potentially shrinks the time dimension effectively by using the more informative spatial features of a higher dimension.

**Backpropogation** Let us consider the derivative of the scalar function  $F$  on  $(l_k)_{k=1}^N$  with respect to path  $x^{\mathcal{D}}$ , given the derivatives of  $F$  with respect to  $(l_k)_{k=1}^N$ . By the Chain rule, it holds that

$$\frac{\partial F((l_1, \dots, l_N))}{\partial x_{t_i}} = \sum_{k=1}^N \frac{\partial F(l_1, \dots, l_N)}{\partial l_k} \frac{\partial l_k}{\partial x_{t_i}}. \quad (15)$$

where  $k \in \{1, \dots, N\}$  and  $i \in \{0, 1, \dots, n\}$ .

If  $t_i \notin [u_{k-1}, u_k]$ ,  $\frac{\partial l_k}{\partial x_{t_i}} = 0$ ; otherwise  $\frac{\partial l_k}{\partial x_{t_i}}$  is the derivative of the single log-signature  $l_k$  with respect to path  $x_{u_{k-1}, u_k}$  where  $t_i \in \mathcal{D} \cap [u_{k-1}, u_k]$ . The log signature  $lS(x^{\hat{\mathcal{D}}})$  with respect to  $x_{t_i}$  is proved differentiable and the algorithm of computing the derivatives is given in [19], denoted by  $\nabla_{x_{t_i}} lS(x^{\hat{\mathcal{D}}})$ . This is the special case for our log-signature layer when  $N = 1$ . In general, for any  $N \in \mathbb{Z}^+$ , it holds that

$$\frac{\partial l_k}{\partial x_{t_i}} = \mathbf{1}_{t_i \in [u_{k-1}, u_k]} \nabla_{x_{t_i}} lS(x_{u_{k-1}, u_k}), \quad (16)$$

where  $i \in \{0, 1, \dots, n\}$  and  $k \in \{1, \dots, N\}$ . Thus the backpropogation algorithm of the log-signature (sequence) layer can be implemented using Equation (15) and (16).<sup>9</sup>

#### 3.2 Logsig-RNN Network

We propose the Logsig-RNN model by incorporating the log-signature layer to the RNN. We defer the motivation of the Logsig-RNN Network to Section 4.

**Model 3.1** (Logsig-RNN Network). *Let  $\mathcal{D} := (u_k)_{k=0}^N$  be a time partition of  $J$ . A Logsig-RNN network computes a mapping from an input path  $x^{\mathcal{D}}$  to an output defined as follows:*

- Compute  $(l_k)_{k=0}^{N-1}$  as the output of the Log-Signature Layer of degree  $M$  for an input  $(x^{\mathcal{D}})$  by Definition 3.1.
- The output layer is computed by  $\mathcal{R}_\sigma((l_k)_{k=0}^{N-1} | \Theta)$ , where  $\sigma$  is a chosen activation function.

**Remark 3.1** (Link between RNN model and Logsig-RNN model). *For  $M = 1$ , Logsig-RNN network is reduced to the RNN model with  $(x_{u_{k+1}} - x_{u_k})_{k=1}^N$  as an input. When  $\mathcal{D}$  coincides with  $\hat{\mathcal{D}}$ , the Logsig-RNN Model is the RNN model with increment of raw data input.*

<sup>9</sup>In iisignature python package, `logsigbackprop(deriv, path, s, Method = None)` returns the derivatives of some scalar function  $F$  with respect to path, given the derivatives of  $F$  with respect to `logsig(path, s, methods)`. Our implementation of the back-propogation algorithm of the log-signature layer uses `logsigbackprop()` provided in iisignature. Readers who are interested in iisignature refer to [20].



**Remark 3.2.** *The sampling time partition of raw data  $\hat{\mathcal{D}}$  can be potentially much higher than  $\mathcal{D}$  used in Logsig-RNN model. The higher frequency of raw data would not increase the dimension of the log-signature layer, but it makes the computation of  $l_k$  more accurate.*

The Logsig-RNN model (depicted in Figure 1) can be served as an alternative to the RNN model and its variants of RNNs, e.g. LSTM, GRU. One main advantage of our method is to reduce the time dimension of the RNN model significantly while using the log-signature as an effective representation of data stream over sub-time interval. It leads to higher accuracy and efficiency compared with the standard RNN model. Compared with Sig-OLR ([21]) our approach may achieve better accuracy via dimension reduction by using the log signature sequence of lower degree to represent the signature of high degree.

### 3.3 LP-Logsig-RNN Network

In many computer vision applications like the gesture recognition, the input path dimension is large, which is typically over 30. The dimension of the truncated (log) signature grows faster w.r.t. the path dimension. It motivates to add a linear projection (embedding) layer to reduce a high dimensional path to a low dimensional path, which is used for the input of the Log-Signature Layer (See Figure 4). The mapping  $L$ , implemented by the embedding layer, translates the input sequence  $(X_{t_i})_{i=1}^n$  into real vectors  $(LX_{t_i})_{i=1}^n$ , where  $LX_{t_i} \in \mathbb{R}^{d'}$  and  $d' < d$ . The weights in the embedding layer are trainable and are learned from data. The addition of the embedding layer effectively leads to significant dimension reduction of the log signature layer to avoid the potential overfitting issue. The proposed algorithm is applied to ChaLearn2013 data in Section 5.3.

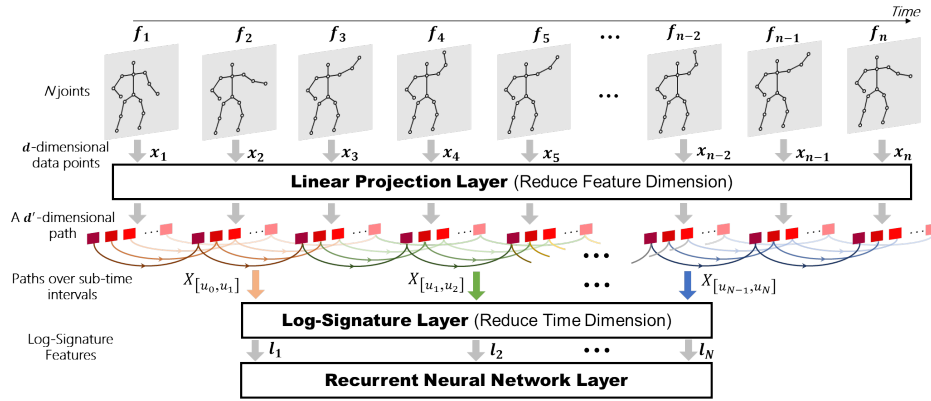


Figure 4: Architecture of LP-Logsig-RNN Model.

## 4 Universality of Logsig-RNN Network

In this section, we prove the universality of Logsig-RNN network to approximate a solution to any controlled differential equation under mild conditions. The motivation of the Logsig-RNN network comes naturally from the numerical approximation theory of the SDEs.

Let  $(X_t)_{t \in [0, T]}$  and  $(Y_t)_{t \in [0, T]}$  be two stochastic processes under the probability space  $(\Omega, \mathcal{F}, P)$  such that  $Y$  is the solution to Equation (17) driven by the path  $X$ ,

$$dY_t = f(Y_t)dX_t, Y_s = \xi, \quad (17)$$

where  $X$  has finite  $p$ -variation a.s., and  $f : \mathbb{R} \rightarrow L(E, \mathbb{R})$  is a smooth vector field satisfying certain regularity condition. Let  $I_f$  denote the solution map which maps  $X_{[0, T]}$  to  $Y_T$ . The goal is to learn the solution map  $I_f$  from the input-output pairs  $(X_{[0, T]}^{(i)}, Y_T^{(i)})_{i=1}^{N_s}$ , which are iid samples of  $(X_{[0, T]}, Y_T)$ .

Classical numerical schemes of simulation of the solution to Equation (17) are mainly composed with two steps:

1. Local Approximation of  $Y_t - Y_s$  when  $t$  is close to  $s$ .
2. Paste the local approximation together to get the global approximation for  $Y_T$ .

Let us start with the local approximation of the solution to Equation (17) using Taylor Expansion. By step  $M$  Taylor Expansion, we have

$$Y_t - Y_s \approx \sum_{k=1}^M f^{\circ k}(Y_s) \int_{s < s_1 < \dots < s_k < t} dX_{t_1} \otimes \dots \otimes dX_{s_k}, \quad (18)$$

where  $f^{\circ m} : \mathbb{R} \rightarrow L(E^{\otimes m}, \mathbb{R})$  is defined recursively by

$$\begin{aligned} f^{\circ 1} &= f; \\ f^{\circ k+1} &= D(f^{\circ k})f, \end{aligned} \quad (19)$$

where  $D(g)$  denotes the differential of the function  $g$ .

We paste the local Taylor approximation together to estimate for the solution on the whole time interval  $[0, T]$ . The strategy is outlined as follows. Fix a time partition  $\mathcal{D} = (u_k)_{k=0}^N$  of  $[0, T]$ . We define the estimator  $(\hat{Y}_{u_k}^{\mathcal{D}, M})_k$  given by  $M$ -step Taylor expansion associated with  $\mathcal{D}$  in the following recursive way: for  $k \in \{0, \dots, N-1\}$ ,

$$\begin{aligned} \hat{Y}_{u_0}^{\mathcal{D}, M} &= y_0, \\ \hat{Y}_{u_{k+1}}^{\mathcal{D}, M} &= \hat{Y}_{u_k}^{\mathcal{D}, M} + \sum_{j=1}^M f^{\circ j}(\hat{Y}_{u_k}^{\mathcal{D}, M}) X_{u_k, u_{k+1}}^j \\ &:= g_{\mathcal{D}, M}^f(l_k, \hat{Y}_{u_k}^{\mathcal{D}, M}), \end{aligned} \quad (20)$$

where  $M$  is the degree of truncated (log)signature,

$$l_k := l_k^M := lS_M(x_{u_k, u_{k+1}}). \quad (21)$$

$\hat{Y}_{u_N}^{\mathcal{D}, M}$  converges to  $Y_T$  when  $\Delta\mathcal{D}$  tends to 0 provided  $f$  is smooth enough. The following theorem provides the bounds of the time mesh  $\Delta\mathcal{D}$  and degree of the log-signature  $M$  to achieve any given error tolerance level  $\varepsilon$ .

**Theorem 4.1** (Global Approximation Theorem). *Let  $\hat{Y}_{u_N}^{\mathcal{D}, M}$  be defined as previously. For any  $\varepsilon > 0$ , when  $\Delta\mathcal{D} \leq \left(\frac{\varepsilon}{C}\right)^{p/([\gamma]+1-p)}$  and  $M \geq \lceil \gamma \rceil$ , then  $\hat{Y}_{u_N}^{\mathcal{D}, M}$  satisfies that*

$$\|Y_T - \hat{Y}_{u_N}^{\mathcal{D}, M}\| \leq \varepsilon, \quad (22)$$

where  $S(X) \in K$ ,  $K$  is a compact set  $S(V_p(J, E))$  and  $C$  is a constant depending  $p, \gamma$ , the norm of  $f$  and the radius of  $K$  defined in Equation (37).

*Proof.* See Appendix B. □

The key observation we make is that there is a remarkable similarity between the recursive structure of an RNN  $\mathcal{R}_\sigma$  and the one defined by the numerical Taylor approximation to solutions of SDEs  $\hat{Y}_{u_N}$  (Figure 5). It is noted that the numerical approximation of the solution  $\hat{Y}_{u_{k+1}}^{\mathcal{D}, M}$  represented in Equation (20) depends on  $\hat{Y}_{u_k}^{\mathcal{D}, M}$  and the log-signature  $l_k$ . In this way,  $\hat{Y}_{u_k}^{\mathcal{D}, M}$  plays a role similar to the hidden neurons of the RNN model with  $(l_k)_{k=0}^{N-1}$  as an input (see Figure 5). It motivates us to propose the Logsig-RNN Network (Model 3.1) to approximate the solution to any SDE under the regularity condition. This idea is natural if one thinks that  $g_{\mathcal{D}, M}^f$  can be universally approximated by neural network. We establish the universality theorem of the Logsig-RNN network as follows.

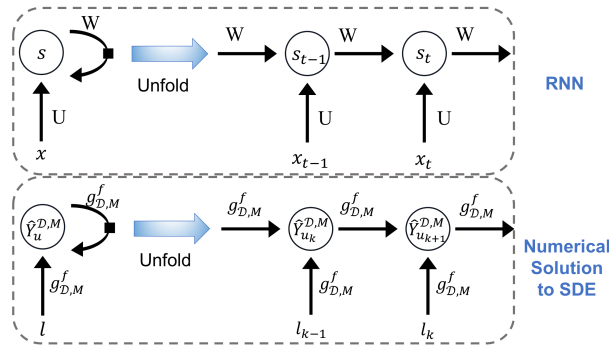


Figure 5: The shared recursive structure of numerical approximation of the solution  $\hat{Y}_{u_N}$  and the RNN  $\mathcal{R}_\sigma$ .

**Theorem 4.2** (Universality of Logsig-RNN Model). *Let  $Y$  denote the solution of a SDE of form (17) under the previous regularity condition of Theorem B.1. Let  $K$  be any a compact set  $S(V_p(J, E))$ . Assume  $f \in C_b^\infty$ <sup>10</sup>. For any  $\varepsilon > 0$ , there exist the constants  $C_1 := C_1(p, \gamma, f, K)$  and  $C_2 := C_2(f, K)$  such that  $M > \lfloor p \rfloor$  and  $\Delta\mathcal{D} \leq \min(\varepsilon^{p/M+1-p}C_1, \varepsilon C_2)$ ,  $l_k$  is defined in Equation (21). Then there exists a RNN  $\mathcal{R}_\sigma(|\Theta)$  with some  $\Theta$ , s.t.*

$$\sup_{S(X) \in K} \|Y_T - \mathcal{R}_\sigma((l_k)_{k=1}^N | \Theta)\| \leq \varepsilon. \quad (23)$$

Before proceeding the proof, we use  $G$  to denote the common recursive structure between those two. Specifically, for any given function  $\tilde{f} : \mathbb{R}^{d+e} \rightarrow \mathbb{R}^e$ , define  $G_{\tilde{f}} := G_{\tilde{f}, o_1, N} : \mathbb{R}^{N \times d} \rightarrow \mathbb{R}^{N \times e}$  as follows:

$$(x_1, \dots, x_N) \mapsto (o_1, \dots, o_N),$$

where  $o_{t+1} = \tilde{f}(x_{t+1}, o_t), \forall t \in \{1, \dots, N-1\}$ . As  $o_1$  is set to be the same and  $N$  is fixed in Theorem 4.2, we skip the subscript  $o_1$  and  $N$  in the notation  $G_{\tilde{f}}$ .

On the one hand, when  $\tilde{f}(x, s) := A\sigma(Ux + Ws)$ , where  $A$  is a matrix of dimension  $d \times e$ ,  $x \in \mathbb{R}^d$  and  $s \in \mathbb{R}^e$ , then  $G_{\tilde{f}}$  is the RNN equipped with the activation function  $\sigma$ , denoted by  $\mathcal{R}(|\Theta)$ ; on the other hand, the numerical solution to SDE  $\hat{Y}_{u_N}$  is  $G_{g_{\mathcal{D}, M}^f}$ . Therefore the error  $E_2$  is the norm of the difference between  $G_{A\sigma(Ux+W)}$  and  $G_{g_{\mathcal{D}, M}^f}$ , i.e.

$$\hat{Y}_{u_N} - \mathcal{R}_\sigma((l_k)_{k=1}^N) = \left( G_{g_{\mathcal{D}, M}^f} - G_{A\sigma(Ux+W)} \right) ((l_k)_{k=1}^N) \quad (24)$$

*Proof.* By the triangle inequality, it holds that

$$\|Y_T - \mathcal{R}_\sigma((l_k)_{k=1}^N | \Theta)\| \leq \underbrace{\|Y_T - \hat{Y}_{u_N}\|}_{E_1} + \underbrace{\|\hat{Y}_{u_N} - \mathcal{R}_\sigma((l_k)_{k=1}^N | \Theta)\|}_{E_2}. \quad (25)$$

By Global Approximation Theorem (Theorem 4.1),  $E_1$  can be arbitrarily small by setting  $\Delta\mathcal{D}$  sufficiently small and truncation degree of the log-signature  $M$  sufficiently large.

The universality of the Logsig-RNN model is reduced to control the error  $E_2$ , which is the difference between  $G_{A\sigma(Ux+W)}$  and  $G_{g_{\mathcal{D}, M}^f}$  (Equation 24). Lemma C.1 ensures that the shallow neural network can approximate any continuous function uniformly well while Lemma C.2 demonstrates the continuity of the map  $\tilde{f} \mapsto G_{\tilde{f}}$ . Combining both lemmas we are able to show that  $E_2$  can be arbitrarily small provided that  $\Delta\mathcal{D}$  sufficiently small and degree  $M$  sufficiently large. The statement and the proof of Lemma C.1 and Lemma C.2 can be found in Appendix C.  $\square$

## 5 Numerical Experiments

We demonstrate the performance of the Logsig-RNN algorithm on both synthetic data (generated by a SDE) and empirical data, including both UCI pen-digit data and gesture data Chalearn 2013 in terms of the accuracy, efficiency and robustness. We benchmark our approach with three methods, i.e. the RNN model with raw data and folded raw data (denoted by  $\text{RNN}_0$  and  $\text{RNN}_{\mathcal{D}}$ <sup>11</sup> resp.) and Sig-OLR.

### 5.1 Synthetic Data Generated by a SDE

We simulate 2000 samples of input-output pairs based on Example 5.1 for  $T = 10$  using the Milstein's method.  $(W_t)_{t \in [0, T]}$  is one-dimensional Brownian motion. We use 80% of data for the training set, and the rest for the testing set. We simulate the sample path using time step  $\frac{T}{1000}$ . For ease of notation, let  $D_n$  denote the equally space time partition of  $[0, T]$  of  $n$  steps. Here  $\hat{\mathcal{D}} = D_{1001}$ .

**Example 5.1.** *Suppose  $Y_t$  satisfies the following SDE:*

$$dY_t = (-\pi Y_t + \sin(\pi t))dX_t^{(1)} + Y_t dX_t^{(2)}, Y_0 = 0. \quad (26)$$

where  $X_t = (X_t^{(1)}, X_t^{(2)}) = (t, W_t)$ , and the integral is in the Stratonovich sense.

<sup>10</sup>  $f \in C_b^\infty$  means  $f$  is infinitely differentiable and all the derivatives are bounded. This regularity condition can be weakened.

<sup>11</sup>  $\text{RNN}_{\mathcal{D}}$  means the RNN model with  $(s_k)_{k=1}^{|D|}$  with  $s_k = (x_{t_i})_{t_i \in [u_k, u_{k+1}]}$  as the input.

**Accuracy Comparison** We compare the accuracy of the predicted solution using Logsig-RNN and  $RNN_{\mathcal{D}}$ .<sup>12</sup> Let maximum number of epochs  $N_e = 25000$  and the MSE is used as the indicator of the goodness of the fitting.<sup>13</sup> Figure 7 shows that Logsig-RNN outperforms significantly  $RNN_{\mathcal{D}}$  in terms of MSE. Table 2 indicates that the log signature is useful for dimension reduction compared with folded raw data for the spatial features of RNN.

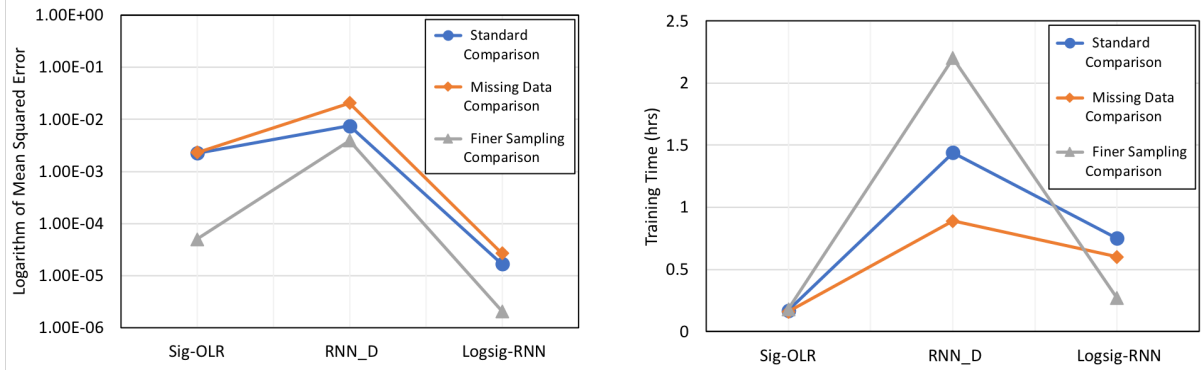


Figure 6: Performance comparison of different methods in different scenarios. Figure (Left) and Figure (Right) are plots of the logarithm of MSE and the training time resp.

N \ M	2	3	4	5	6	$RNN_{\mathcal{D}}$
2	(2, 2)	(2, 5)	(2, 8)	(2, 14)	(2, 23)	(2, 500)
4	(4, 2)	(4, 5)	(4, 8)	(4, 14)	(4, 23)	(4, 250)
8	(8, 2)	(8, 5)	(8, 8)	(8, 14)	(8, 23)	(8, 125)
Sig-OLR	(1, 3)	(1, 7)	(1, 15)	(1, 31)	(1, 63)	

Table 2: Feature dimension comparison. The default method is Logsig-RNN model. The 1<sup>st</sup> and 2<sup>rd</sup> coordinates are time dimension and spatial dimension resp.

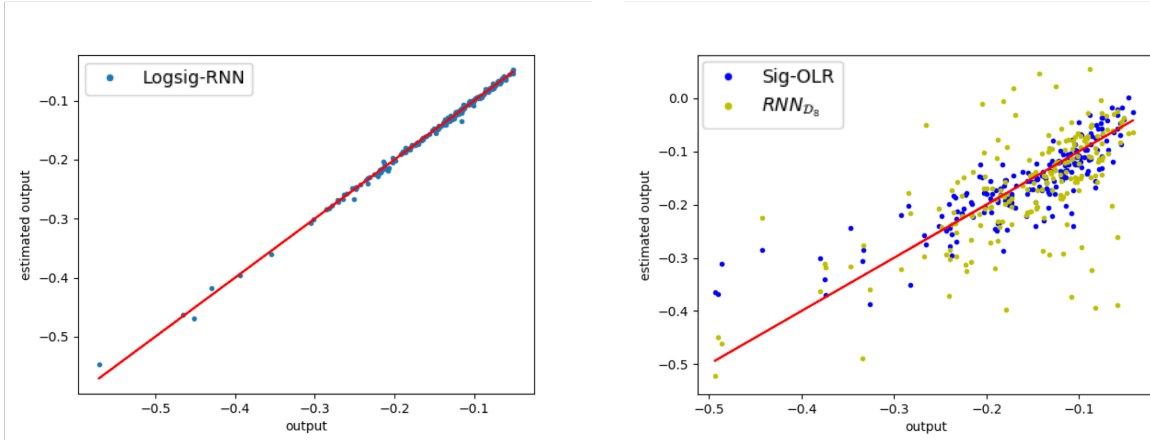


Figure 7: The comparison plot of estimated output v.s the actual output for the testing set.  $M = 6$  and  $N = 8$ .

**Efficiency Analysis** Given the error tolerance  $\epsilon = 2 \times 10^{-6}$ , we compare the efficiency of these methods in terms of the training time until the loss function reaches  $\epsilon$ . Figure 8 records the logarithm of MSE for Logsig-RNN model with different  $M$  and  $N$ . In Figure 6, the 'Standard Comparison' displays that Logsig-RNN outperforms all the baseline methods in terms of the accuracy significantly (Figure 7) and it reduces the training time of  $RNN_{\mathcal{D}}$  by 1/3. It is expected that Logsig-RNN takes longer training time as Logsig-RNN uses the RNN model instead of linear model used by Sig-OLR.

<sup>12</sup>Here we do not include the result for  $RNN_0$  in this SDE example as it performs too badly compared with the other methods.

<sup>13</sup>We implement the algorithm using in Tensorflow. It runs on a Windows 10 computer with processor 2.60 GHz Intel Core i5, and memory 8 GB. The optimizer is chosen to Adam optimizer with learning rate  $\alpha = 0.0001$ .

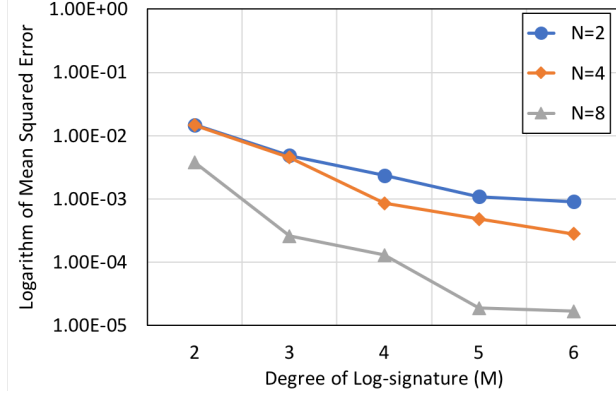


Figure 8: The sensitivity analysis of Logsig-RNN model.

**Robustness to missing data** To mimic the missing data case, for each sample input path, we randomly throw away 5% points. In Figure 6, the grey curve shows that Our method reduces the MSE of the testing set significantly compared with  $RNN_{\mathcal{D}}$  for the missing data case.

**High sampling frequency of input path** Here we consider two experiments regarding changing sampling frequency of the input path (HF sampling). In the first experiment, we simulate the SDE data using different time mesh  $\Delta\hat{\mathcal{D}}$ , while in the second experiment, we use the SDE data simulated using finest time mesh  $\Delta_{5000}$  as the underlying data stream, and down-sample it at different time mesh  $\Delta\hat{\mathcal{D}}$ .

Let  $\Delta\hat{\mathcal{D}}$  be  $\frac{T}{1000}$ ,  $\frac{T}{2500}$  and  $\frac{T}{5000}$  respectively. For the first experiment, Figure 9 shows that Logsig-RNN performs better when the sampling frequency of the raw data is higher. When  $\Delta\hat{\mathcal{D}}$  is larger, the signature of the raw data  $x^{\hat{\mathcal{D}}}$  is more accurate to the signature of the underlying path  $x$ , without increasing the feature dimension. It gives better prediction than the RNN due to reduction of time dimension of RNN significantly. In Figure 6, it shows that the marginal improvement of the proposed method is more significant for the finer sampling case.

In the second experiment, when the sampling frequency of input data is higher, the smaller MSE is for both methods. But it is noted that our proposed Logsig-RNN method outperforms consistently and significantly both in terms of out-of-sample accuracy. Furthermore, in terms of the training time,  $RNN_0$  has the significant growth in training time with respect to the sampling frequency, while that of our method is almost the same for different frequency<sup>14</sup> (Figure 10).

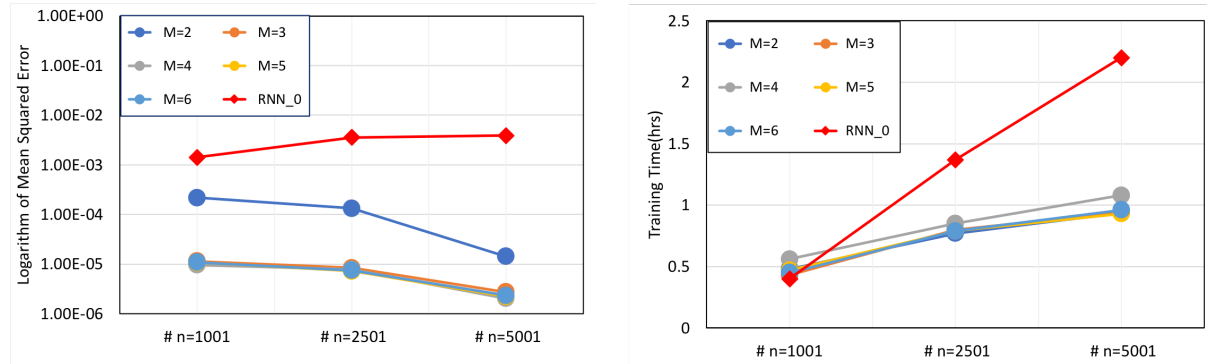


Figure 9: First experiment on HF sampling: Here  $|\hat{\mathcal{D}}| = 1001, 2501$  and  $5001$ . The left is comparison of logarithm of MSE, and the right is of training time. Here  $N = 4$ .

<sup>14</sup>The training time of our method includes the computation time of log-signature sequence of the input path.

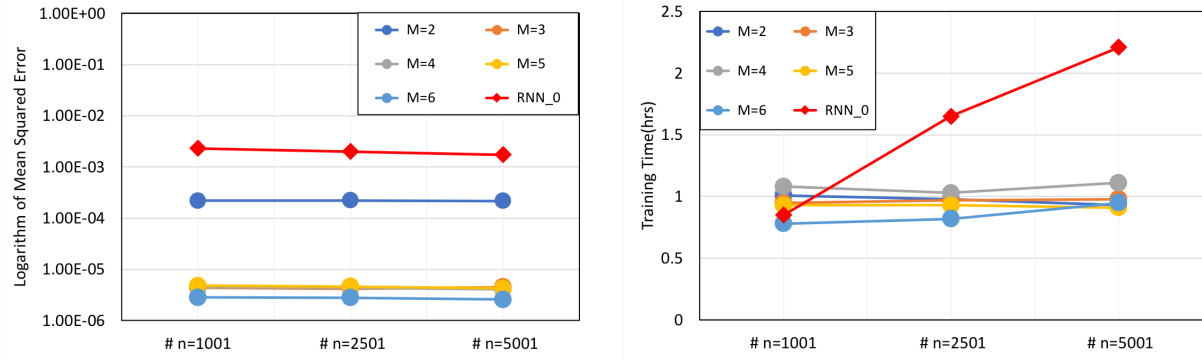


Figure 10: Second experiment on HF sampling: Here  $|\hat{\mathcal{D}}| = 1001, 2501$  and  $5001$ . The left is comparison of logarithm of MSE, and the right is of training time. Here  $N = 4$ .

### 5.2 UCI Pen-Digit Data

In this section, we apply the Logsig-RNN algorithm on the UCI sequential pen-digit data<sup>15</sup>. In Table 3, the Logsig-RNN with  $M = 4$  and  $N = 4$  achieves the accuracy 97.88% in the testing data compared with 95.80% of  $RNN_0$  and the accuracy 88.62% of  $RNN_{\mathcal{D}}$ . In addition, the training time of the Logsig-RNN takes 30% of  $RNN_{\mathcal{D}}$  and 3% of the training time of  $RNN_0$ .

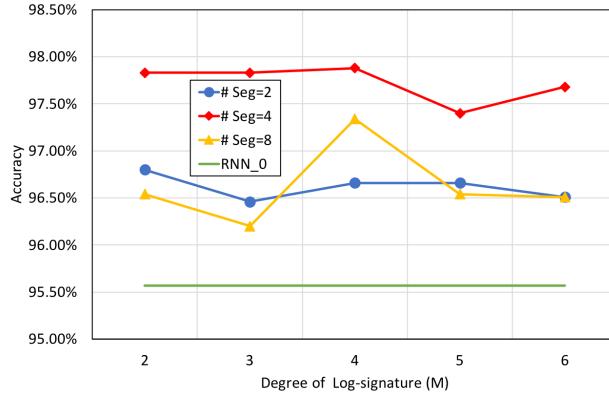


Figure 11: The accuracy comparison of Logsig-RNN in the testing set. The accuracy of  $RNN_{\mathcal{D}}$  is below 89%.

**Robustness to missing data and change of sampling frequency** To mimic the missing data case, we randomly throw a certain portion of points for each sample, and evaluated the trained models of Logsig-RNN and  $RNN_0$  to the new testing data. Table 3 shows that our proposed method outperforms the other methods significantly for the missing data case. Figure 12 shows the robustness of trained Logsig-RNN model for the down-sampled test data. Here the test data is down-sampled to that of length 8 provided in UCI data. For  $M = 4$ , the accuracy of testing data is above 80%, which is about 4 times of that of the baseline methods.

r \ M	2	3	4	5	6	$RNN_0$
0%	97.83%	97.83%	97.88%	97.40%	97.68%	95.80%
10%	97.63%	97.77%	97.14%	96.88%	97.60%	40.91%
20%	96.74%	97.06%	96.68%	95.85%	97.06%	37.28%
30%	95.99%	95.40%	95.17%	95.03%	95.77%	32.65%

Table 3: The accuracy of the modified testing set using different missing data rate ( $r$ ). Here  $N = 4$ .

<sup>15</sup><https://archive.ics.uci.edu/ml/datasets/Pen-Based+Recognition+of+Handwritten+Digits>

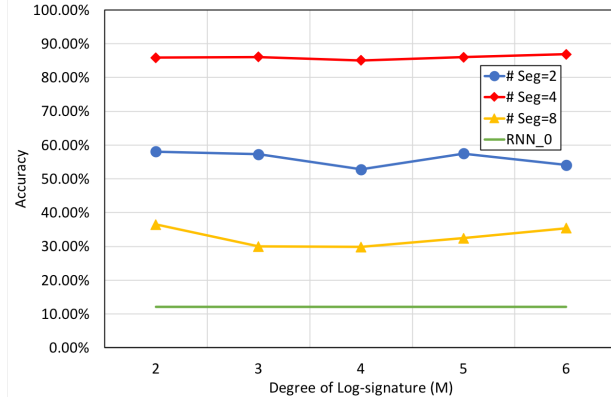


Figure 12: Validation of the trained models on the down-sampled dataset. The accuracy of  $RNN_{\mathcal{D}}$  is below 13.5%

### 5.3 Gesture Data: Chalearn 2013

The Chalearn 2013 dataset [10] is a public available dataset for gesture recognition, which contains 20 Italian gestures performed by 27 subjects. It provides Kinect data, which contains RGB, depth, foreground segmentation and skeletons. Here, we only skeleton data (20 3D joints) for the gesture recognition task. The skeletons are pre-processed by first subtracting the central joint, which is the average position of all joints in one sample. Then we normalize the data and sample all clips to 39 frames by linear interpolation and uniform sampling. We apply LP-Logsig-RNN algorithm depicted in Figure 4 with a customized cumulative sum layer followed by the log-signature transformation with  $d' = 30$ . We add DropOut layer to both of the linear projecting layer and LSTM layer to avoid over-fitting, where the first dropout rate is 0.3 and the second is 0.5. The number of hidden neurons of LSTM layer is 128. To make fair comparison, a DropOut layer is added to the benchmark  $RNN_0$ .

**Comparison with the State-of-the-art** We compare our method with several state-of-the-art methods which only used the skeleton data [22]. Table 4 shows that the Logsig-RNN algorithm with  $M = 2$  and  $N = 4$  outperforms other methods in terms of the accuracy of 10-folded cross validation. We present both the results with and without the data-augmentation. With data-augmentation, our results significantly outperform other methods to achieve the state-of-the-art result.

Method	Accuracy(%)	Data Augmentation
Deep LSTM [35]	87.10	—
Two-stream LSTM [38]	91.70	✓
ST-LSTM (Tree) + Trust Gate [24]	92.00	✓
3s_net_TTM [23]	92.08	✓
$RNN_0$	90.92	✗
$RNN_0$ (+data augmentation)	91.18	✓
<b>LP-Logsig-RNN</b>	<b>92.21</b>	✗
<b>LP-Logsig-RNN</b> (+data augmentation)	<b>92.85</b>	✓

Table 4: Comparison of methods on the Chalearn 2013 data.

**Robustness to missing data** We randomly set a certain percentage of frames ( $r$ ) by all-zeros for each sample in the validation set, and evaluate the trained models of our method and  $RNN_0$  to the new validation data. Table 5 shows that logsig-RNN model with  $M = 2$  consistently beats the baseline  $RNN_0$  for different  $r$ , which validates the robustness of our method comparing with the benchmark.

## 6 Conclusion

In conclusion, the Logsig-RNN model, inspired from the numerical approximation theory of SDEs, provides an accurate, efficient and robust algorithm on supervised learning problems on the path space. Numerical results show that it outperforms Sig-OLR,  $RNN_0$  and  $RNN_{\mathcal{D}}$  on both synthetic data and empirical data. In ChaLearn2013 skeleton data, LP-Logsig-RNN achieves the state-of-the-art classification accuracy. In future, we will investigate applications of the Logsig-RNN in the sequence-to-sequence learning tasks.

r \ M	2	3	4	RNN <sub>0</sub>
0%	92.37%	89.66%	70.71%	90.09%
10%	91.32%	88.58%	69.11%	81.77%
20%	90.33%	86.60%	67.89%	68.22%
30%	87.68%	81.74%	63.24%	50.35%
50%	74.40%	57.13%	41.07%	21.78%

Table 5: The accuracy of the testing set with missing data with different ratio ( $r$ ). Here  $N = 4$ .

## References

- [1] J. P. Bishwal. *Parameter estimation in stochastic differential equations*. Springer, 2007. 3
- [2] F. Black and M. Scholes. The pricing of options and corporate liabilities. *Journal of political economy*, 81(3):637–654, 1973. 3
- [3] H. Boedihardjo, X. Geng, T. Lyons, and D. Yang. The signature of a rough path: Uniqueness. *arXiv preprint arXiv:1406.7871*, 2014. 5
- [4] T. Q. Chen, Y. Rubanova, J. Bettencourt, and D. K. Duvenaud. Neural ordinary differential equations. In *Advances in neural information processing systems*, pages 6571–6583, 2018. 1
- [5] I. Chevyrev and A. Kormilitzin. A primer on the signature method in machine learning. *arXiv preprint arXiv:1603.03788*, 2016. 5
- [6] R. R. Coifman, I. G. Kevrekidis, S. Lafon, M. Maggioni, and B. Nadler. Diffusion maps, reduction coordinates, and low dimensional representation of stochastic systems. *Multiscale Modeling & Simulation*, 7(2):842–864, 2008.
- [7] J. C. Cox and S. A. Ross. The valuation of options for alternative stochastic processes. *Journal of financial economics*, 3(1-2):145–166, 1976. 3
- [8] A. S. Dickinson. Optimal approximation of the second iterated integral of brownian motion. *Stochastic Analysis and Applications*, 25(5):1109–1128, 2007.
- [9] D. L. Donoho et al. High-dimensional data analysis: The curses and blessings of dimensionality. *AMS math challenges lecture*, 1(2000):32, 2000. 2
- [10] S. Escalera, J. González, X. Baró, M. Reyes, O. Lopes, I. Guyon, V. Athitsos, and H. J. Escalante. Multi-modal gesture recognition challenge 2013: dataset and results. In *ICMI*, 2013. 15
- [11] P. Friz, P. Gassiat, and T. Lyons. Physical brownian motion in a magnetic field as a rough path. *Transactions of the American Mathematical Society*, 367(11):7939–7955, 2015. 3
- [12] P. Friz and N. Victoir. *Multidimensional Stochastic Processes as Rough Paths: Theory and Applications*. Cambridge Studies in Advanced Mathematics. Cambridge University Press, 2010. 19
- [13] K.-i. Funahashi and Y. Nakamura. Approximation of dynamical systems by continuous time recurrent neural networks. *Neural networks*, 6(6):801–806, 1993. 1
- [14] C. W. Gardiner et al. *Handbook of stochastic methods*, volume 3. springer Berlin, 1985. 3
- [15] B. Graham. Sparse arrays of signatures for online character recognition. *arXiv preprint arXiv:1308.0371*, 2013. 3
- [16] L. G. Gyurkó, T. Lyons, M. Kontkowski, and J. Field. Extracting information from the signature of a financial data stream. *arXiv preprint arXiv:1307.7244*, 2013. 3
- [17] B. Hambly and T. Lyons. Uniqueness for the signature of a path of bounded variation and the reduced path group. *Annals of Mathematics*, 171(1):109–167, 2010. 5
- [18] S. Hochreiter and J. Schmidhuber. Long short-term memory. *Neural computation*, 9(8):1735–1780, 1997.
- [19] R. Jeremy. *Iterated-Integral Signatures in Machine Learning*. PhD thesis, 2019. 8
- [20] R. Jeremy and G. Benjamin. The iisignature library: efficient calculation of iterated-integral signatures and log signatures. *arXiv preprint arXiv:1802.08252*, 2018. 8
- [21] D. Levin, T. Lyons, and H. Ni. Learning from the past, predicting the statistics for the future, learning an evolving system. *arXiv preprint arXiv:1309.0260*, 2013. 3, 4, 5, 9
- [22] C. Li, X. Zhang, and L. Jin. Lpsnet: a novel log path signature feature based hand gesture recognition framework. In *Proceedings of the IEEE International Conference on Computer Vision*, pages 631–639, 2017. 3, 15
- [23] C. Li, X. Zhang, L. Liao, L. Jin, and W. Yang. Skeleton-based gesture recognition using several fully connected layers with path signature features and temporal transformer module. *CoRR*, abs/1811.07081, 2018. 15
- [24] J. Liu, A. Shahroudy, D. Xu, A. C. Kot, and G. Wang. Skeleton-based action recognition using spatio-temporal lstm network with trust gates. *IEEE Transactions on Pattern Analysis and Machine Intelligence*, 40(12):3007–3021, Dec 2018. 15



- [25] Y. Lu, A. Zhong, Q. Li, and B. Dong. Beyond finite layer neural networks: Bridging deep architectures and numerical differential equations. *arXiv preprint arXiv:1710.10121*, 2017. [1](#)
- [26] T. Lyons, T. Lévy, and M. Caruana. *Differential Equation driven by Rough Paths*. Springer, 2006. [4](#), [5](#), [6](#), [7](#), [18](#)
- [27] T. Lyons, H. Ni, and H. Oberhauser. A feature set for streams and an application to high-frequency financial tick data. In *Proceedings of the 2014 International Conference on Big Data Science and Computing*, page 5. ACM, 2014. [3](#)
- [28] T. J. Lyons. Differential equations driven by rough signals. *Revista Matemática Iberoamericana*, 14(2):215–310, 1998. [2](#)
- [29] R. C. Merton et al. Theory of rational option pricing. *Theory of Valuation*, pages 229–288, 1973. [3](#)
- [30] T. Mikolov, M. Karafiát, L. Burget, J. Černocký, and S. Khudanpur. Recurrent neural network based language model. In *Eleventh Annual Conference of the International Speech Communication Association*, 2010.
- [31] H.-G. Müller, R. Sen, and U. Stadtmüller. Functional data analysis for volatility. *Journal of Econometrics*, 165(2):233–245, 2011. [4](#)
- [32] H. Palangi, L. Deng, Y. Shen, J. Gao, X. He, J. Chen, X. Song, and R. Ward. Deep sentence embedding using long short-term memory networks: Analysis and application to information retrieval. *IEEE/ACM Transactions on Audio, Speech and Language Processing (TASLP)*, 24(4):694–707, 2016.
- [33] A. Papavasiliou, C. Ladroue, et al. Parameter estimation for rough differential equations. *The Annals of Statistics*, 39(4):2047–2073, 2011. [3](#)
- [34] J. Reizenstein and B. Graham. The iisignature library: efficient calculation of iterated-integral signatures and log signatures. *arXiv preprint arXiv:1802.08252*, 2018. [3](#)
- [35] A. Shahroudy, J. Liu, T.-T. Ng, and G. Wang. Ntu rgb+d: A large scale dataset for 3d human activity analysis. 06 2016. [15](#)
- [36] B. W. Silverman et al. Smoothed functional principal components analysis by choice of norm. *The Annals of Statistics*, 24(1):1–24, 1996. [4](#)
- [37] R. R. Viorio, B. Shuai, J. Lu, D. Xu, and G. Wang. A siamese long short-term memory architecture for human re-identification. In *European Conference on Computer Vision*, pages 135–153. Springer, 2016.
- [38] H. Wang and L. Wang. Modeling temporal dynamics and spatial configurations of actions using two-stream recurrent neural networks. *2017 IEEE Conference on Computer Vision and Pattern Recognition (CVPR)*, pages 3633–3642, 2017. [15](#)
- [39] E. Weinan. A proposal on machine learning via dynamical systems. *Communications in Mathematics and Statistics*, 5(1):1–11, 2017. [1](#)
- [40] Z. Xie, Z. Sun, L. Jin, H. Ni, and T. Lyons. Learning spatial-semantic context with fully convolutional recurrent network for online handwritten chinese text recognition. *IEEE transactions on pattern analysis and machine intelligence*, 40(8):1903–1917, 2018. [3](#)
- [41] W. Yang, T. Lyons, H. Ni, C. Schmid, L. Jin, and J. Chang. Leveraging the path signature for skeleton-based human action recognition. *arXiv preprint arXiv:1707.03993*, 2017. [3](#)

## Appendix A Preliminary of Rough Paths Theory

### A.1 The algebraic properties of the (log)-signature

If  $F_1$  and  $F_2$  are two linear subspaces of  $T((E))$ , let us denote by  $[F_1, F_2]$  the linear span of all the elements of the form  $[a, b]$ , where  $a \in F_1$  and  $b \in F_2$ . Consider the sequence  $(L_n)_{n \geq 0}$  be the subspace of  $T((E))$  defined recursively as follows:

$$L_0 = 0; \forall n \geq 1, L_n = [E, L_{n-1}]. \quad (27)$$

**Definition A.1.** *The space of Lie formal series over  $E$ , denoted as  $\mathcal{L}((E))$  is defined as the following subspace of  $T((E))$ :*

$$\mathcal{L}((E)) = \{l = (l_0, \dots, l_n, \dots) | \forall n \geq 0, l_n \in L_n\}. \quad (28)$$

Theorem 2.3 can be rewritten in the following form.

**Theorem A.1** (Theorem 2.23 [26]). *Let  $X$  be a path of finite 1-variation. Then the log-signature of  $X$  is a Lie series in  $\mathcal{L}((E))$ .*

#### A.1.1 Real-valued functions on the signatures of paths.

We now introduce a special class of linear forms on  $T((E))$ ; Suppose  $(e_1^*, \dots, e_d^*, \dots)$  are elements of  $E^*$ . We can introduce coordinate iterated integrals by setting  $X^{(i)}_u := \langle e_i^*, X_u \rangle$ , and rewriting  $\langle e_{i_1}^* \otimes \dots \otimes e_{i_n}^*, S(X) \rangle$  as the scalar iterated integral of coordinate projection. In this way, we realize  $n^{\text{th}}$  degree coordinate iterated integrals as the restrictions of linear functionals in  $E^{\otimes n}$  to the space of signatures of paths. If  $(e_1, \dots, e_d)$  is a basis for a finite dimensional space  $E$ , and  $(e_1^*, \dots, e_d^*)$  is a basis for the dual  $E^*$ . Therefore, it follows that

$$\mathbf{X}_J = \sum_{k \geq 0} \sum_{i_1, \dots, i_k \in \{1, 2, \dots, d\}} \int \dots \int_{\substack{u_1 < \dots < u_k \\ u_1, \dots, u_k \in J}} dX_{u_1}^{(i_1)} \otimes \dots \otimes dX_{u_k}^{(i_k)} e_1 \otimes \dots \otimes e_k.$$

### A.2 The kernel of the signature transformation

The definition of the tree-like path is given as follows.

**Definition A.2** (Tree-like Path). *A path  $X : J = [S, T] \rightarrow E$  is tree-like if there exists a continuous function  $h : J \rightarrow [0, +\infty)$  such that  $h(S) = h(T) = 0$  and such that, for all  $s, t \in J$  with  $s \leq t$ ,*

$$\|X_t - X_s\| \leq h(s) + h(t) - 2 \inf_{u \in [s, t]} h(u).$$

### A.3 Rough Path and the Extension Theory

Let  $C_{0,p}(\Delta_T, T^{\lfloor p \rfloor}(E))$  be the space of all continuous functions from the simplex  $\Delta_T := \{(s, t) | 0 \leq s \leq t \leq T\}$  into the truncated tensor algebra  $T^{\lfloor p \rfloor}(E)$ . We define the  $p$ -variation metric on this linear space as follows: for  $X, Y \in C_{0,p}(\Delta_T, T^{\lfloor p \rfloor}(E))$ , set

$$d_p(X, Y) = \max_{1 \leq i \leq \lfloor p \rfloor} \left( \sup_{\mathcal{D} \subset [0, T]} \sum_{\mathcal{D}} \|X_{t_{i-1}, t_i}^i - Y_{t_{i-1}, t_i}^i\|^{\frac{p}{i}} \right)^{\frac{1}{p}}. \quad (29)$$

**Definition A.3.** *Let  $p \geq 1$  be a real number and  $n \geq 1$  be an integer. Let  $\omega : [0, T] \rightarrow [0, \infty]$  be a control. Let  $X : \Delta_T \rightarrow T^{(n)}$  be a multiplicative functional. We say that  $X$  has finite  $p$ -variation on  $\Delta_T$  controlled by  $\omega$  if*

$$\|X_{s,t}^i\| \leq \frac{\omega(s, t)^{\frac{i}{p}}}{\beta(\frac{i}{p})!}, \forall (s, t) \in \Delta_T. \quad (30)$$

*In general, we say that  $X$  has finite  $p$ -variation if there exists a control such that the conditions above are satisfied.*

The concept of the rough path theory is a generalization of the signature of a path of finite 1-variation.

**Definition A.4** (Rough path). *Let  $E$  be a Banach space. Let  $p \geq 1$  be a real number. A  $p$ -rough path in  $E$  is a multiplicative functional of degree  $\lfloor p \rfloor$  in  $E$  with finite  $p$ -variation. The space of  $p$ -rough paths is denoted by  $\Omega_p(V)$ .*

**Definition A.5** (Geometric rough path). A geometric  $p$ -rough path is a  $p$ -rough path that can be expressed as a limit of 1-rough path in the  $p$ -variation distance defined above. The space of geometric  $p$ -rough path in  $E$  is denoted by  $G\Omega_p(E)$ .

**Theorem A.2** (Extension theorem). Let  $X$  and  $Y$  be two multiplicative functional in  $T^{(n)}(V)$  of finite  $p$ -variation,  $n \geq \lfloor p \rfloor$  controlled by  $\omega$ . Suppose that for some  $\varepsilon \in (0, 1)$ ,

$$\|X_{s,t}^i - Y_{s,t}^i\| \leq \varepsilon \frac{\omega(s,t)^{\frac{i}{p}}}{\beta \left(\frac{i}{p}\right)!}, \quad (31)$$

for  $i = 1, \dots, n$  and for all  $(s, t) \in \Delta_T$ . Then provided  $\beta$  is chosen such that

$$\beta \geq 2p^2 \left( 1 + \sum_{r=3}^{\infty} \left( \frac{2}{r-2} \right)^{\frac{\lfloor p \rfloor}{p}} \right). \quad (32)$$

## Appendix B Proof of Theorem 4.1

**Lemma B.1.** Let  $K$  be a compact set of  $G\Omega_p(J, E)$  for some  $p \geq 1$ .  $J'$  is a compact sub-time interval of  $J$ . Then the mapping  $F : K \rightarrow T^{\lfloor p \rfloor}(E)$ , i.e.  $x \mapsto \log(x_{J'})$  is continuous. The image of  $K$  under the function  $F$  is compact.

**Theorem B.1.** [12] Assume that  $X = (1, X^1, \dots, X^{\lfloor p \rfloor})$  is a  $p$ -geometric rough path<sup>16</sup>. Let  $f$  be a  $Lip(\gamma)$  vector field where  $\gamma > p$ . Then there exists  $C := C(p, \gamma)$  such that

$$\|Y_T - \hat{Y}_{u_N}^{\mathcal{D}, M}\| \leq C \sum_{k=1}^N |f|_{\circ\gamma}^{\lfloor \gamma \rfloor + 1} \|X\|_{p\text{-var}; [t_{k-1}, t_k]}^{\lfloor \gamma \rfloor + 1}. \quad (33)$$

Now we are ready to prove Theorem 4.1.

*Proof.* According to Theorem B.1, there exists  $C := C(p, \gamma)$  such that

$$\|Y_T - \hat{Y}_{u_N}^{\mathcal{D}, M}\| \leq C \sum_{k=1}^N |f|_{\circ\gamma}^{\lfloor \gamma \rfloor + 1} \|X\|_{p\text{-var}; [t_{k-1}, t_k]}^{\lfloor \gamma \rfloor + 1}. \quad (34)$$

It implies that the estimation error is of order  $\Delta^{\frac{\lfloor \gamma \rfloor + 1}{p}}$ . As  $S(X) \in K$ , then it exists a constant  $C_1 > 0$  s.t.

$$\sup_{S(X) \in K} \|X\|_{p\text{-var}, J} \leq C_1. \quad (35)$$

Equation (34) implies that

$$\|Y_T - \hat{Y}_{u_N}^{\mathcal{D}, M}\| \leq \tilde{C} \Delta^{\frac{\lfloor \gamma \rfloor + 1}{p} - 1}. \quad (36)$$

where  $C := C(p, \gamma)$  is given in Theorem B.1 and

$$\tilde{C} = C \max_{k=1}^N \left( \|f\|_{\circ\gamma}^{\lfloor \gamma \rfloor + 1} \right) C_1^p. \quad (37)$$

□

## Appendix C Auxiliary Lemmas for the proof of Theorem 4.2

In the following, we use the uniform norm of a function  $\tilde{f} : K \rightarrow \mathbb{R}^d$ , i.e.

$$\|\tilde{f}\|_{\infty, K} := \sup_{x \in K} |\tilde{f}(x)|.$$

The following lemma on the universality of shallow neural network was proved by Funahshi (1989).

<sup>16</sup>A geometric  $p$ -rough path is the limit of the sequence of the signature of paths of finite 1-variation in the  $p$ -variation distance. A discrete time series of finite length is an example of geometric  $p$ -rough path  $\forall p \geq 1$ .

**Lemma C.1.** Let  $\sigma(x)$  be a sigmoid function (i.e. a non-constant, increasing, and bounded continuous function on  $\mathbb{R}$ ). Let  $K$  be any compact subset of  $\mathbb{R}^n$ , and  $f : K \rightarrow \mathbb{R}^e$  be a continuous function mapping. Then for an arbitrary  $\varepsilon > 0$ , there exist an integer  $N > 0$ , an  $m \times N$  matrix  $A$  and an  $N$  dimensional vector  $\theta$  such that

$$\max_{x \in K} |f(x) - A\sigma(Bx + \theta)| < \varepsilon,$$

holds where  $\sigma : \mathbb{R}^N \mapsto \mathbb{R}^N$  is a sigmoid mapping defined by

$$\sigma'(u_1, \dots, u_N) = (\sigma(u_1), \dots, \sigma(u_N)).$$

**Lemma C.2.** Let  $K$  be any compact subset of  $\mathbb{R}^d$ . Let  $f$  and  $\tilde{f}$  be two continuously differentiable functions on  $\mathbb{R}^{d+e}$ . Then it follows that

$$\|G_f - G_{\tilde{f}}\|_{\infty, K} < C \|f - \tilde{f}\|_{\infty, K},$$

where  $C$  is a constant depending on the  $\nabla f$  and  $N$ , i.e.

$$C = \begin{cases} \frac{C_1^N - 1}{C_1 - 1}, & \text{if } C_1 \neq 1; \\ N, & \text{if } C_1 = 1. \end{cases} \quad (38)$$

$$C_1 := \sup_{(x_1, \dots, x_N) \in K} \max_{k=1}^N \|\nabla_o f(x_k, o_k)\|.$$

*Proof.* As  $f$  and  $\tilde{f}$  are continuous functions and  $K$  is compact, then the image of  $G_f$  and  $G_{\tilde{f}}$  for any  $(x_1, \dots, x_N) \in K$  are compact. Let  $(h_i)_{i=1}^N$  and  $(\tilde{h}_i)_{i=1}^N$  denote  $G_f$  and  $G_{\tilde{f}}$  evaluated at  $(x_1, x_2, \dots, x_N)$  respectively. Then we have

$$h_{i+1} = f(x_{i+1}, h_i) \text{ and } \tilde{h}_{i+1} = \tilde{f}(x_{i+1}, \tilde{h}_i).$$

Then it follows that

$$\begin{aligned} \|h_{i+1} - \tilde{h}_{i+1}\| &= \|f(x_{i+1}, h_i) - \tilde{f}(x_{i+1}, \tilde{h}_i)\| \\ &\leq \|f(x_{i+1}, h_i) - f(x_{i+1}, \tilde{h}_i)\| + \|f(x_{i+1}, \tilde{h}_i) - \tilde{f}(x_{i+1}, \tilde{h}_i)\| \\ &\leq \|f(x_{i+1}, h_i) - \tilde{f}(x_{i+1}, \tilde{h}_i)\| + \sup_{x \in K} \|Df(x, h)\| \|h_i - \tilde{h}_i\|, \end{aligned}$$

which shows the recursive relation of  $\|h_i - \tilde{h}_i\|$ .

It is easy to check that if  $a_{i+1} \leq C_0 + C_1 a_i$  with  $a_0 = 0$ , it implies that

$$a_i \leq \begin{cases} \frac{C_1^i - 1}{C_1 - 1} C_0, & \text{if } C_1 \neq 1 \\ i C_0, & \text{if } C_1 = 1. \end{cases}$$

Therefore using the above inequality when  $a_i = \|h_i - \tilde{h}_i\|$ ,  $C_0 = \max_{x \in K} \|f - \tilde{f}\|$ , it follows that

$$\|h_i - \tilde{h}_i\| \leq C \|f - \tilde{f}\|_{\infty},$$

and so does

$$\|G_f - G_{\tilde{f}}\|_{\infty, K} \leq C \|f - \tilde{f}\|_{\infty, K},$$

where  $C$  is defined by Equation (38). □